Solubility of $Mo_6S_{4.5}I_{4.5}$ Nanowires in Common Solvents: A Sedimentation Study

Valeria Nicolosi,[†] Daniel Vrbanic,[‡] Ales Mrzel,[‡] Joe McCauley,[†] Seán O'Flaherty,[§] Cormac McGuinness,[†] Giuseppe Compagnini,[||] Dragan Mihailovic,[‡,⊥] Werner J. Blau,[†] and Jonathan N. Coleman*[,†]

Department of Physics, University of Dublin, Trinity College, Dublin 2, Ireland, Jozef Stefan Institute, Jamova 39, 1000 Ljubljana, Slovenia, European Synchrotron Radiation Facility ESRF, Grenoble, France, Chemistry Department, University of Catania, Viale A. Doria 6, 95125, Catania, Italy, and Mo6, Teslova 30, 1000 Ljubljana, Slovenia

Received: October 22, 2004; In Final Form: January 24, 2005

Due to their ease of fabrication and monodisperse, metallic nature, molybdenum-sulfur-iodine nanowires are an interesting alternative to carbon nanotubes for some applications. However very little is known about the solubility of these materials. In this work we have investigated the solubility of $Mo_6S_{4.5}I_{4.5}$ nanowire soot in a range of common solvents by performing sedimentation studies and microscopic and spectroscopic characterization. A sedimentation equation was derived showing that the concentration of any insoluble dispersed phase decreases exponentially with time. We find that in all solvents, $Mo_6S_{4.5}I_{4.5}$ nanowire soot contains three phases, two of which are insoluble with one stable phase. Microscopy and spectroscopy show that the first insoluble phase is associated mainly with spherical impurities and sediments rapidly out of solution resulting in purification. The second phase appears to consist of insoluble nanowire bundles and sediments more slowly, eventually leaving a stable dispersion of nanowire bundles. The stably dispersed bundles tend to be smaller than their insoluble counterparts. The best solvents studied were 2-propanol and dimethylformamide. Microscopy studies showed that, in the case of 2-propanol, sonication significantly reduced the bundle size relative to the unsonicated bulk. However, during sedimentation, large quantities of bundles were observed to reaggregate to form larger bundles which subsequently sedimented out of solution. In general, the sedimentation properties of the various phases did not vary significantly with concentration indicating that the insoluble nanowires are intrinsically insoluble. However, the diameter of the stably dispersed bundles decreased with concentration, until very small bundles consisting of only two or three nanowires were observed at concentrations below 0.003 mg/mL. In addition, stable composite dispersions were produced by mixing the nanowires with poly(vinylpyrrolidone) in 2-propanol opening the way for the formation of polymer/inorganic nanowire composites.

1. Introduction

One-dimensional nanostructures such as carbon nanotubes (CNTs) have generated much excitement among materials scientists in recent years.[1−4] However difficulties associated with their lack of solubility and homogeneity have long been a problem.[5−12]

In view of these issues some attention is now moving to other one-dimensional, inorganic alternatives. Many interesting reports on the successful synthesis of nanostructured binary or ternary inorganic one-dimensional objects have been reported in recent literature.[13−17] Molybdenum-chalcogenide nanowires are, in particular, a new class of one-dimensional objects possessing functional properties very similar to the CNTs but with some significant advantages. Of these, the most important are the fact that the synthesis is straightforward and accessible to scale-up and that these materials tend to be monodisperse with all nanowires having identical electronic properties. These advantages alone are significant. The most promising of these inorganic materials are the family of nanowires made up of molybdenum, sulfur and iodine (MoSI). These materials are produced with stoichiometries described by $Mo_6S_{9-x}I_x$.[17] Easy fabrication, monodisperse diameters and metallic behavior are some of their qualities. These materials display excellent field emission properties[18] in addition to remarkable mechanical stiffness and low shear modulus.[19] Furthermore, the novel chemical structure of these materials makes them an obvious target for chemical functionalization.

However, issues such as the optimum solvent, the maximum solubility, the nanowire bundling process and the stabilization of the dispersions by mixing with a polymeric matrix have not been studied. In this paper we present a quantitative study of the dispersion properties of $Mo_6S_{4.5}I_{4.5}$ nanowires in a range of common solvents. This is done by monitoring the optical transmission of the dispersion as a function of time. These data can be transformed to represent variations in the local solid-phase concentration as nonsoluble phases sediment out of solution. In addition we suggest a model to describe the sedimentation process for a given phase.

Using these techniques, we determine the best solvents and the maximum solubility of nanowires in each. Furthermore we use electron microscopy and spectroscopy to characterize the nature of both the dispersed material and the sediment, showing

* Corresponding author e-mail: colemaj@tcd.ie.
[†] University of Dublin.
[‡] Jozef Stefan Institute.
[§] European Synchrotron Radiation Facility ESRF.
[||] University of Catania.
[⊥] Mo6.

10.1021/jp045166r CCC: $30.25
Published on Web 03/26/2005

that any impurity material present in the MoSI powder sediments out of solution relatively quickly. While this process results in purification we also note that a significant fraction of the nanowires in each sample are also nonsoluble. To investigate this further we have monitored the sedimentation of MoSI in 2-propanol as a function of nanowire concentration. As the concentration is decreased, no significant increase in the fraction of stably dispersed nanowires was observed. Finally, varying amounts of polyvinylpyrollidone were added to MoSI dispersions in 2-propanol. While this tended to increase the fraction of stably dispersed material, the increase tended to be mainly in the form of impurities.

2. Experimental Methods

$Mo_6S_{9-x}I_x$ nanowires were fabricated by direct synthesis from elemental material that had been mixed in the desired stoichiometries.[17] Depending on the initial quantities of material used in the synthetic step, it is possible to obtain two different kinds of nanowires, having different stoichiometries: $Mo_6S_3I_6$ or $Mo_6S_{4.5}I_{4.5}$. In both cases the final material is a powder composed of aggregates of individual nanowires, each having a diameter of 0.94 nm.[17]

In the work presented here, dispersions of the $Mo_6S_{4.5}I_{4.5}$ nanowires were prepared by mixing the MoSI powder in various solvents. In addition dispersions were made in 2-propanol for a range of concentrations from 1 to 3×10^{-3} mg/mL. Furthermore composite dispersions were fabricated by mixing MoSI powder with poly(vinylpyrrolidone) (PVP) in 2-propanol at a range of MoSI/PVP mass ratios. In all cases the dispersions were initially sonicated for 2 min using a high power ultrasonic tip (120 W, 60 kHz) followed by a mild sonication for 2 h using a low power ultrasonic bath. For each sample the dispersion was then transferred to a 1 cm quartz cuvette. Sedimentation studies were carried out by monitoring the transmission of laser pulses ($\lambda = 650$ nm, pulse duration 10 ms) through the center of the sample over the course of 200 h. This was carried out 4 times, and the results were averaged. The transmission was then transformed into turbidity using the Lambert−Beer law

$$I/I_0 = e^{-Tl}$$

where I/I_0 is the transmittance, T is the turbidity and l is the sample length. The turbidity can be thought of as the product of the sample concentration, C, and an effective extinction coefficient, α, which represents all absorption and scattering processes.[23]

Field emission scanning electron microscopy (SEM) studies have been performed using a Hitachi S-4300 on uncoated powder samples. Transmission electron microscopy studies were carried out on nanowire dispersions at different concentrations using a Hitachi H-7000. Deposition of the prepared dispersions on the Formvar coated copper grids (mesh size 300) was performed by simple drop casting in ambient conditions. In addition, high-resolution TEM (HRTEM) characterization was carried out using a FEI Tecnai F20 Field emission microscope and holey carbon grids. Absorption measurements were made using a Perkin-Elmer Lambda 900 UV−vis−NIR spectrometer. XPS spectra were obtained using a Kratos Axis HS and Mg K_α X-ray source.

3. Sedimentation Theory

To fully understand the sedimentation of nonsoluble phases in MoSI dispersions we need to derive an equation to describe the local concentration of sedimenting particles as a function of time. To do this we consider the sedimentation of solid particles under the assumptions[20−22] that 1) the solid particles are small with respect to the sedimentation vessel and all have the same density, 2) the constituents of the solution are incompressible, and 3) there is no mass transfer between the solid and the fluid phases during sedimentation. Under these circumstances the dynamic process of a particulate system can be described by field variables that must obey the two local conservation equations for mass and linear momentum[20−22]

$$\frac{\partial C}{\partial t} + \nabla(C v_s) = 0 \tag{1}$$

$$\rho_S \frac{\partial}{\partial t}(C v_S) + \rho_S \nabla(C v_S^2) = -\nabla(C p_f) - C\rho_s g + \beta \nabla C \tag{2}$$

where C is the local concentration of the sedimenting phase under study, ρ_s is the solid component density, v_s is the velocity of the solid component, p_f is the fluid pressure, g is the acceleration due to gravity and β is related to the solid fluid interaction force and has the dimensions of a pressure. In addition we note that the fluid pressure obeys $-dp_f\, dz = \rho_l g$.

Solution of the above equations gives

$$\frac{\partial C}{\partial t} = \frac{-Cg(\rho_s - \rho_l)v_s - \rho_s C v_s dv_s/dt}{(\beta - p_f)} \tag{3}$$

To eliminate v_s and dv_s/dt we need to consider Newton's second law. The forces acting on a single particle are gravity and the viscous drag force. Thus we can write

$$m\frac{dv_S}{dt} = mgb - f v_S \tag{4}$$

where m is the mass per sedimentation particle, b is the buoyancy correction factor ($b=1-\rho_l/\rho_s$) and f is the frictional coefficient as given by Stokes law. Solving this equation gives

$$v_S = \frac{mgb}{f}(1 - e^{-(f/m)t}) \tag{5}$$

and

$$\frac{dv_S}{dt} = gbe^{-(f/m)t} \tag{6}$$

We can estimate m and f from the known properties of the system. Using these quantities we can calculate that, for this system, the exponential decays over the order of seconds. As this is a very short time compared to the time scale of the sedimentation experiment, the exponentials can be neglected. Integration of eq 3 then gives

$$C = C_n \exp\left[-\frac{g^2(\rho_S - \rho_l)mb}{f(\beta - p_f)}t\right] = C_n e^{-t/\tau} \tag{7}$$

where C_n is a constant and

$$\tau = \frac{f(\beta - p_f)}{g^2(\rho_S - \rho_l)mb} \tag{8}$$

For spherical particles, $f = 6\pi\eta a$, where η is the solvent viscosity, a is the particle radius and $m = 4\rho_s\pi a^3/3$. This allows us to express the time constant as

$$\tau_{spherical} = \frac{9\eta(\beta - p_f)}{2g^2(\rho_s - \rho_l)^2 a^2} \quad (9)$$

However, in the case of cylindrical particles, the frictional coefficient tends to be higher than for the spherical case. For a cylindrical particle of length, *l*, and radius *r*, the viscous drag is given by, $f = 6K\pi\eta a$, where *K* is the drag coefficient, which is a function of l/r.[23] *K* tends to increase with aspect ratio, approaching 5 for aspect ratios of 1000. In addition $m = \rho_s \pi r^2 l$ and $a = (3r^2 l/4)^{1/3}$. Thus the time constant for cylindrical particles is

$$\tau_{cylindrical} = \frac{6K\eta(\beta - p_f)}{g^2(\rho_s - \rho_l)^2 (r^2 l)^{2/3}} \left(\frac{3}{4}\right)^{1/3} \quad (10)$$

In a real dispersion there may be more than one distinct sedimenting phases. Each phase will be characterized by its own time constant and by the partial concentration of that phase. In addition there may be a soluble component. Thus the local time dependent concentration of a dispersion with *n* insoluble phases and one soluble phase is described by the equation

$$C(t) = C_0 + \sum_n C_n e^{-t/\tau_n} \quad (11)$$

where C_0 is the concentration of the soluble phase. In addition conservation of mass dictates that the total initial concentration, C_{Tot}, is given by

$$C_{Tot} = C_0 + \sum_n C_n \quad (12)$$

In this experiment we monitor the total turbidity, $T(t) = \alpha C(t)$. Applying eq 11 shows that the turbidity should decay as

$$T(t) = T_0 + \sum_n T_n e^{-t/\tau_n} = \alpha_0 C_0 + \sum_n \alpha_n C_n e^{-t/\tau_n} \quad (13)$$

where α_0 and α_n represent the extinction coefficients of the soluble and the insoluble phases, respectively. Thus the analogue of eq 12 is

$$T_{Tot} = T_0 + \sum_n T_n \quad (14)$$

4. Results and Discussion

4.1. Sedimentation Studies. *4.1.1. Solvent Dependence.* To determine the optimum solvent to disperse $Mo_6S_{4.5}I_{4.5}$ nanowires, sedimentation studies were carried out on dispersions of the nanowires in a range of solvents, 2-propanol (IPA), dimethyl formamide (DMF), dimethyl sulfoxide (DMSO), chloroform, water, acetone and ethanol, all at a concentration of 0.1 mg/mL. These data are presented in Figure 1 as the local turbidity in the center of the sample bottle as a function of time. In all cases the turbidity at zero time is equal to the total initial turbidity (T_{Tot}) but tends to fall off as time passes as material sediments out of solution. Finally, for very long times, the local turbidity tends to a constant value which represents the turbidity associated with the stably dispersed material in each solvent.

For each solvent the rate of sedimentation and the turbidity associated with stably dispersed material is different, leading to different sedimentation curves. It is immediately clear, however, that the curves at the top right of the graph represent the best solvents. From this it is clear that IPA and DMF are far superior solvents to acetone and ethanol for example.

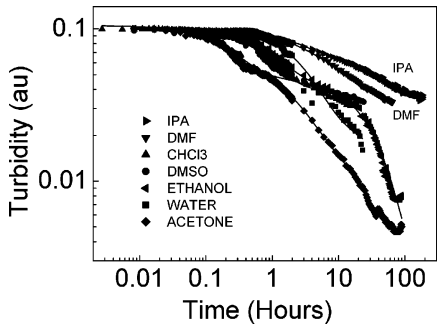

Figure 1. Experimental sedimentation curves (symbols) and biexponential fits (continuous lines) for $Mo_6S_{4.5}I_{4.5}$ nanowire bundles dispersed in various solvents at a concentration of 0.1 mg/mL.

To extract quantitative information the sedimentation curves must be fit to eq 13. In all cases it was found that the best fit occurred for one stably dispersed component and two insoluble components (n=2 in eq 13). The fits are shown as the solid lines in Figure 1. For all samples five fit parameters could be extracted, T_0, T_1, τ_1, T_2 and τ_2. These are presented in Table 1.

Of these, the most important is T_0, as this relates to the partial concentration of stably dispersed material. As we have discussed previously, in all cases the stable fraction consists of bundles of nanowires. From the data in Table 1, it is clear that IPA, DMF, DMSO and chloroform are the best solvents with T_0/T_{Tot} values of 31%, 33%, 31% and 29% respectively. Conversely, water, acetone and ethanol are relatively poor solvents.

Turning to phases 1 and 2 we note that the time constants vary significantly over the range of solvents. This is because for any sedimenting particle, the time constant varies with the solvent viscosity and density. It can be shown that both τ_1 and τ_2 vary approximately as $\eta/(\rho_s - \rho_l)^2$ for the solvents studied as predicted by eqs 8 and 9.

It should be pointed out at this stage that there is a possibility that the observed stable phase may in fact be a sedimenting phase with a very long time constant. However, even if this is the case, this phase is stable over a time frame of at least 200 h. This is easily enough time to carry out any solution based sample preparation or characterization. This means that whether this material is truly soluble or not, it certainly has significant advantages over materials such as CNTs which are unstable in all common solvents.

4.1.2. Purification by Sedimentation. For all solvents except water, $\tau_1 < \tau_2$, meaning that phase 1 tends to sediment more rapidly. To determine the nature of phases 1 and 2 we compute the sedimentation curves for phases 1 and 2 in 2-propanol. These are presented in Figure 2 with the experimental sedimentation curve and the fit for comparison. These clearly show that phases 1 and 2 have almost completely sedimented from solution by approximately 13 and 200 hours, respectively.

To identify the nature of the phases, a high concentration dispersion of 40.2 mg of $Mo_6S_{4.5}I_{4.5}$ nanowire material in 13.5 mL of 2-propanol (3 mg/mL) was prepared. This dispersion was allowed to sediment for 13 h before decantation to separate the sediment (sediment 1) which was expected to contain mostly phase 1. The remaining dispersion was resonicated and allowed sediment for a further 200 h before decantation to separate the sediment (sediment 2, mostly phase 2) from the solute (phase 0). For all three phases the samples were dried and weighed. The masses of sediment 1, sediment 2 and the solute were found to be 26.1, 7.5 and 4.6 mg, respectively (2 mg of powder was unrecoverable). This means that approximately 12% of the material is stably dispersed with a solubility of at least 0.34

TABLE 1: Fit Parameters Obtained from Fitting the Various Sedimentation Curves Described in the Text to Eq 11 for One Stably Dispersed and Two Insoluble Components[a]

solvent	T_0/T_{Tot} (%)	T_1/T_{Tot} (%)	τ_1 (hours)	T_2/T_{Tot} (%)	τ_2 (hours)	D_{Before} (nm)	D_{After} (nm)	L_{Before} (mm)	L_{After} (mm)	NW	Imp
IPA	31 ± 6	30 ± 2	2.3 ± 0.5	39 ± 5	38 ± 3.5	8.3 ± 0.4	6.2 ± 3	5.25 ± 0.3	3.5 ± 0.2	Y	N
DMF	33 ± 2	29 ± 5	2.6 ± 0.2	38 ± 2	18 ± 1.5	9.6 ± 1.72	8.9 ± 3	5.1 ± 2.5	4.6 ± 3.1	Y	N
DMSO	31 ± 5	55 ± 4	0.74 ±0.1	21 ± 5	21 ± 7	16 ± 10				N	Y
chloroform	29 ± 4	56 ± 8	0.3 ± 0.2	26 ± 6	7.0 ± 1.5	21 ± 21	18 ± 32	3.3 ± 2	3.1 ± 2.8	Y	T
water	13 ± 9	47 ± 6	6.0 ± 3	43 ± 6	6.0 ± 3	145 ± 89	95 ± 88	5.9 ± 4	5.4 ± 7	Y	Y
acetone	7 ± 1	51 ± 5	0.26 ± 0.1	45 ± 4	4.2 ± 0.8	70 ± 80	67 ± 94	9.8 ± 6.3	9.2 ± 7	Y	T
ethanol	4 ± 2	52 ± 4	0.9 ± 0.15	47 ± 1	32 ± 3	17 ± 7	17 ± 9	5.7 ± 3.5	6.1 ± 5	Y	T

concentration, nanowires in IPA (mg/mL)	T_0/T_{Tot} (%)	T_1/T_{Tot} (%)	τ_1 (hours)	T_2/T_{Tot} (%)	τ_2 (hours)	D_{Before} (nm)	D_{After} (nm)
0.1	32 ± 4	30 ± 305	2.3 ± 0.5	39 ± 5	38 ± 4.5	8.4 ± 2.2	5.5 ± 3
0.05	33 ± 7	31 ± 3.5	4 ± 1.5	37 ± 2.5	35 ± 2.5	8.3 ± 1.7	5.3 ± 3
0.025	33 ± 6	34 ± 3.5	8 ± 0.6	36 ± 7.5	83 ± 2.5	7.9 ± 1.4	4.9 ± 3
0.0125	43 ± 7	20 ± 5	3.3 ± 0.7	40 ± 6	35 ± 1.5	7.7 ± 0.8	5.3 ± 3

nanowire/PVP ratio	T_0/T_{Tot} (%)	T_1/T_{Tot} (%)	τ_1 (hours)	T_2/T_{Tot} (%)	τ_2 (hours)
1/1	26 ± 8	42 ± 7.5	7.5 ± 2.5	46 ± 10	37 ± 11
1/3	34 ± 10	41 ± 9.5	17 ± 3	34 ± 12	86 ± 79
1/30	52 ± 7	23 ± 6.5	18.5 ± 3	23 ± 9	17 ± 3
1/10	47 ± 8	26 ± 9.5	9.5 ± 2.1	31 ± 6	79 ± 46
1/100	61 ± 6	28 ± 12.5	17 ± 20	37 ± 18	3.5 ± 2

[a] The upper and middle parts of the table describe the data obtained from the solvent and concentration dependent studies, respectively, while the lower part describes the data for the samples with a range of polymer-nanowire mass ratios. Column 2 describes the partial turbidity of the soluble component as a percentage of the total MoSI turbidity. Similarly columns 3 and 5 describe the partial turbidity of the impurity phase and of the insoluble nanowire phase respectively as a percentage of the total MoSI turbidity. Columns 4 and 6 contain the time constants relevant to each of these phases. Columns 7, 8, 9 and 10 show the measured bundle diameter and length respectively before and after sedimentation. Column 11 indicates the presence or absence of both nanowires and impurities in the solution after sedimentation.

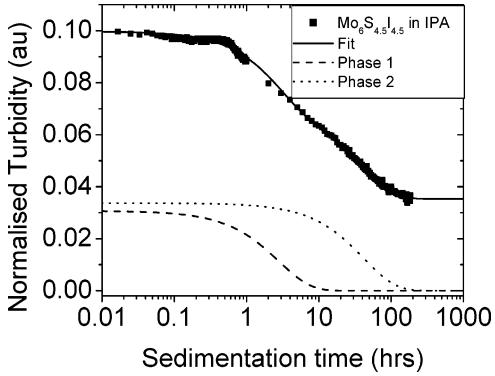

Figure 2. Normalized turbidity as a function of sedimentation time for $Mo_6S_{4.5}I_{4.5}$ powder dispersed in 2-propanol (0.1 mg/mL). The solid line is a fit to eq 6 with two insoluble phases and one stably dispersed phase. The dashed and dotted lines are the computed decay curves for (insoluble) phases 1 and 2, respectively.

mg/mL. This is significant as this concentration is high enough for solution based composite formation to be technologically useful.

4.1.3. Investigation of Separated Phases. To investigate the nature of the phases, SEM was carried out on each phase as well as the raw material for comparison. Representative images are shown in Figure 3 for A) undispersed $Mo_6S_{4.5}I_{4.5}$ powder, B) sediment 1, C) sediment 2 and D) the solute. The undispersed powder contains large numbers of large nanowire bundles and significant amounts of particulate impurity materials. Similarly, sediment 1 also contains large bundles with large numbers of impurities. In contrast, sediment 2 contains many bundles but significantly fewer impurities. Finally the solute material contains large numbers of small diameter bundles with very few impurities.

To further examine the difference between the phases, a small portion of each phase (and the raw material for comparison) was redissolved in 2-propanol at a concentration of 0.1 mg/mL. Immediately after dissolution, UV−vis−NIR absorption spectra were measured for each solution over the range 0.5−5 eV. These are presented in Figure 4. The spectrum for sediment 1 is reasonably featureless over the measured range. In contrast the spectra representing sediment 2 and the solute are similar with peaks at 0.63, 0.85, 1.73 and 2.67 eV. This strongly suggests that these phases contain the same materials. As we know from the SEM (see above) and TEM (see below) studies that the solute consists predominately of nanowire bundles, it is likely that these features are associated with nanowire optical transitions. This means that not only does the solute contain large amounts of nanowires but also a significant proportion of sediment 2 is in the form of (insoluble) nanowires. In addition there are suggestions that the 0.63 and 1.73 eV nanowire features may be present in the sediment 1 spectrum. This is consistent with the fact that some nanowire bundles were observed in the SEM micrographs for sediment 1. Finally the spectrum for the as produced material appears to be a convolution of the individual phases as expected.

X-ray photoemission spectroscopy (XPS) was also used to investigate the chemical differences between the three separated powders (the two sedimenting ones and the solute) as well as the raw material (spectra not shown). The powders were mounted on silicon dioxide substrates and discounting the XPS peaks from the substrate the spectra were analyzed to determine the atomic concentration of the constituents. The total atomic stoichiometries were determined as being the following: $Mo_{0.31}S_{0.49}I_{0.20}$ for the as-synthesized material, $Mo_{0.3}S_{0.58}I_{0.12}$ for sediment 1, $Mo_{0.44}S_{0.38}I_{0.18}$ for sediment 2 and $Mo_{0.47}S_{0.32}I_{0.21}$ for the solute. The estimated error in the atomic concentration is about 5%. It is clear from these results that sediment 1 is significantly different from the other two phases. While phase 1 appears to be mainly constituted by MoS_2 with traces of interpolated iodine, phase 2 and the solute appear to be very close do the given stoichiometry $Mo_6S_{4.5}I_{4.5}$ ($Mo_{0.4}S_{0.3}I_{0.3}$). This

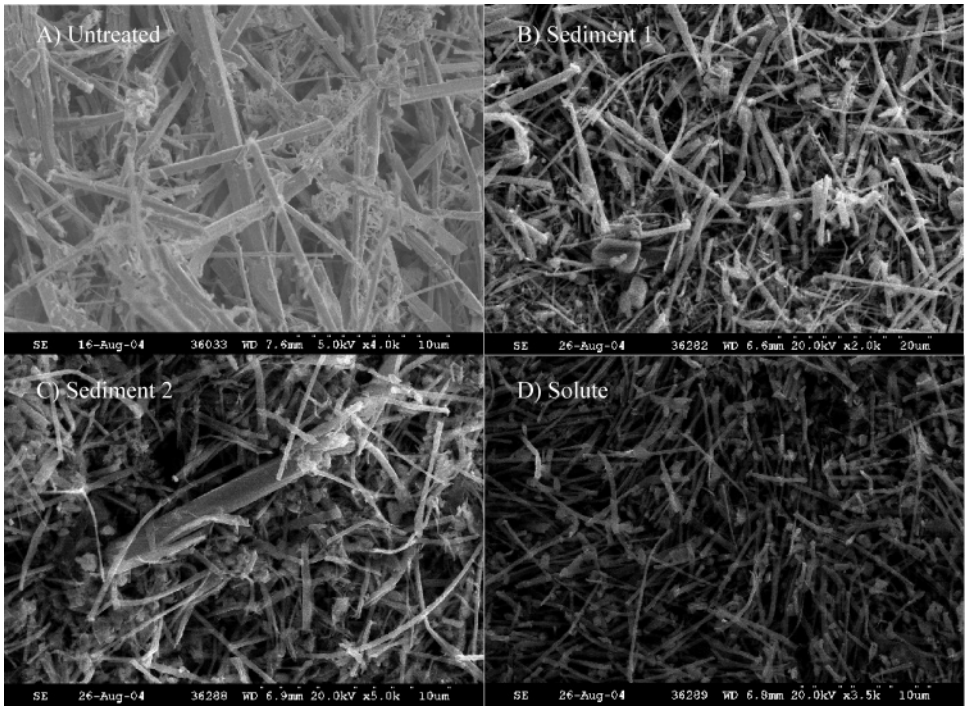

Figure 3. Scanning electron microscopy images of A) raw, undispersed $Mo_6S_{4.5}I_{4.5}$ powder, B) sediment 1, C) sediment 2 and D) the solute. Note the relative lack of impurities and small bundle size in the solute sample.

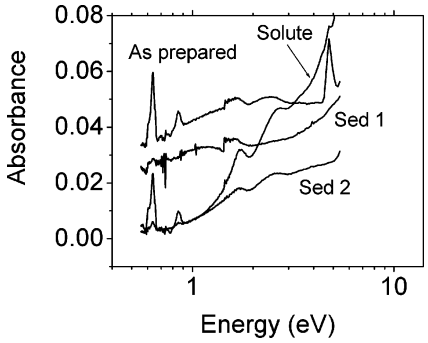

Figure 4. UV−vis−NIR absorption spectra for solutions of as prepared $Mo_6S_{4.5}I_{4.5}$ powder, sediment 1, sediment 2 and the solute. The solutions were prepared by redispersing the material from the separated phases. In all cases the concentration was 0.1 mg·mL.

offers further confirmation of the purification of the material by the sedimentation process.

From these results, it is clear that this impurity material sediments out over a shorter time scale than the insoluble nanowires. However, it is not evident why some of the nanowire material is also insoluble. However, a reasonable quantity of the material is stable in the form of small diameter nanowire bundles. This clearly shows that sedimentation is a simple method for producing pure, stable dispersions of $Mo_6S_{4.5}I_{4.5}$ nanowires. This method is comparable to methods previously used for carbon nanotubes.[8]

4.2. Characterization by TEM. *4.2.1. Solvent Dependence.* Transmission electron microscopy has been used to investigate the morphological properties of $Mo_6S_{4.5}I_{4.5}$ nanowire bundles before, during and after sedimentation. For this purpose as-synthesized $Mo_6S_{4.5}I_{4.5}$ nanowires were dispersed in all solvents used in the sedimentation study with total initial concentration, $C_{Tot} = 0.1$ mg/mL, and sonicated as described previously. Immediately after sonication, a drop of the dispersion was deposited in a TEM grid for analysis. The dispersion was then allowed to sediment for 100 hours. By this time, a sediment could clearly be seen at the bottom of each sample bottle. This sediment was separated from the stable solution by careful decantation. At this point a drop of the decanted solution was deposited onto a TEM grid for analysis.

For all solvents, both bundles of nanowires and impurities were observed in solution before sedimentation. An example, in this case for the 2-propanol solution, is shown in Figure 5a. In general the impurity material was pseudospherical with diameters in the region of 100 nm. In all cases the dimensions of the nanowire bundles were measured and are presented as average diameters and lengths in Table 1. Presedimentation diameters vary from approximately 8.3 ± 0.4 nm in the case of 2-propanol to 145 ± 89 nm for water. Furthermore bundles lengths varied from 3.3 ± 2.0 μm to 9.8 ± 6.3 μm for chloroform and acetone, respectively. It should be pointed out that these bundle sizes observed before sedimentation are extremely small compared with the bundles present in the as-produced powder. Before sonication the powder consists of extremely large bundles with diameters between 30 and 1000 nm and lengths of many microns. This clearly shows that during sonication the bundles are efficiently broken up. However the bundle size immediately after sonication varies widely with the solvent showing that the solvent choice is an important parameter not only for solvation but also for debundling.

TEM measurements were also made after 100 hours of sedimentation for all solvents. In this case TEM measurements provide evidence of sedimentation based purification or lack of, depending on the solvent. These results are presented in columns 11 and 12. In the column labeled "NW", Y means nanowires were observed, while N signifies that no nanowires were observed after sedimentation. In the column marked "Imp" the same symbols indicate the presence or absence of impurities. However an additional symbol, T, signifies the presence of trace amounts of impurities.

After sedimentation, significant amounts of impurity material were observed in the DMSO and water based dispersions. In addition trace amounts of impurities were found in the chloro-

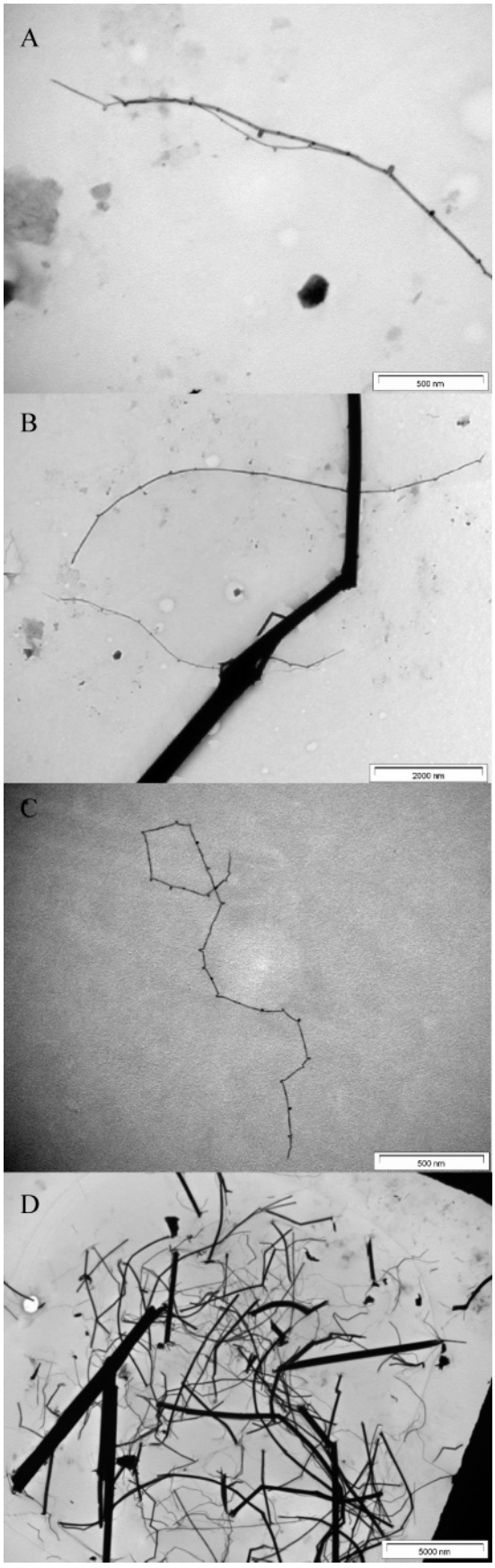

Figure 5. TEM images of material pipetted from the top of the dispersion A) immediately after sonication, B) after 16 h sedimentation, and C) after 96 h sedimentation. Figure 4D) shows material collected from the bottom of the sample vessel after 96 h sedimentation.

form, acetone and ethanol dispersions. Only in the case of IPA and DMF dispersions were no impurities found after 100 hours of sedimentation. In contrast significant quantities of nanowires were observed in all solvents except DMSO after sedimentation. This suggests that in the case of DMSO all the nanowires sedimented out of solution as phase 1 or 2. It should be emphasized at this point that the only solvents to display purification and retain large amounts of nanotubes after sedimentation were 2-propanol and DMF.

The diameters and lengths of a large number of bundles were measured for each solvent after sedimentation and are presented in Table 1. Postsedimentation diameters vary from approximately 6.2 ± 3 nm in the case of 2-propanol to 95 ± 88 nm for water. Furthermore bundles lengths varied from 3.1 ± 2.8 μm to 9.2 ± 7.0 μm for chloroform and acetone, respectively. For all solvents except ethanol both average bundle diameter and length were smaller after sedimentation compared to before. This suggests that sedimentation may be associated with the larger bundles. This possibility is explored below.

4.2.2. Measurement of Aggregation during Sedimentation Process. To further clarify the sedimentation process, experiments were carried out to probe the nature of the nanowire bundles during sedimentation. To this end a 0.1 mg/mL dispersion in 2-propanol was prepared. Immediately after sonication, a very small amount of the dispersion was carefully pipetted from the top of the bottle and deposited on a TEM grid. This was repeated while the sample was sedimenting after 1, 4, 8, 16, 32 and 96 h. In addition a TEM grid was prepared with a sample of the sediment after 96 h.

Representative TEM images for the samples taken from the top of the sample bottle at $t = 0$, $t = 16$ and $t = 96$ h as well as a sediment image are shown in Figure 5. For the $t = 0$ sample the nanowires are present in the form of bundles similar to those found in samples of carbon SWNT. In addition it can clearly be seen that a large number of spherical nanoparticles are present. The average diameter of these particles was measured to be 84 ± 46 nm. These materials can be considered to be an impurity phase. After 16 h, while both small and larger bundles were seen, virtually no impurity material was observed. After 96 h however, only small diameter bundles are present with no sign of impurities. This shows that the sedimentation process is a useful method for the purification of $Mo_6S_{4.5}I_{4.5}$ dispersions. One curious point is the presence of a large number of kinks along the length of the bundles. These were observed in almost every bundle. Further work is underway to understand the nature of these apparent structural defects.

For comparison, a TEM image of the sediment is presented in Figure 5d. Two things are clear from this image. First, a significant proportion of the sediment is in the form of spherical impurities. The rest of the material is composed of bundles of nanowires. However the dimensions of these bundles are significantly larger than those observed in the solution before and after sedimentation, with diameters varying from 30 to 1000 nm. In addition it should be pointed out that the spherical impurities in the sediment have an average diameter of $\sim$900 nm. This strongly suggests that impurities aggregate either during sedimentation or while on the bottom of the sample bottle.

To understand the processes occurring during sedimentation, the diameters and lengths were measured for a large number of bundles from each sedimentation time quoted above. The diameters are presented as histograms in Figure 6. Immediately after sonication, the bundle diameters follow a narrow distribution centered on 7.5 nm and extending up to 40 nm. It is clear

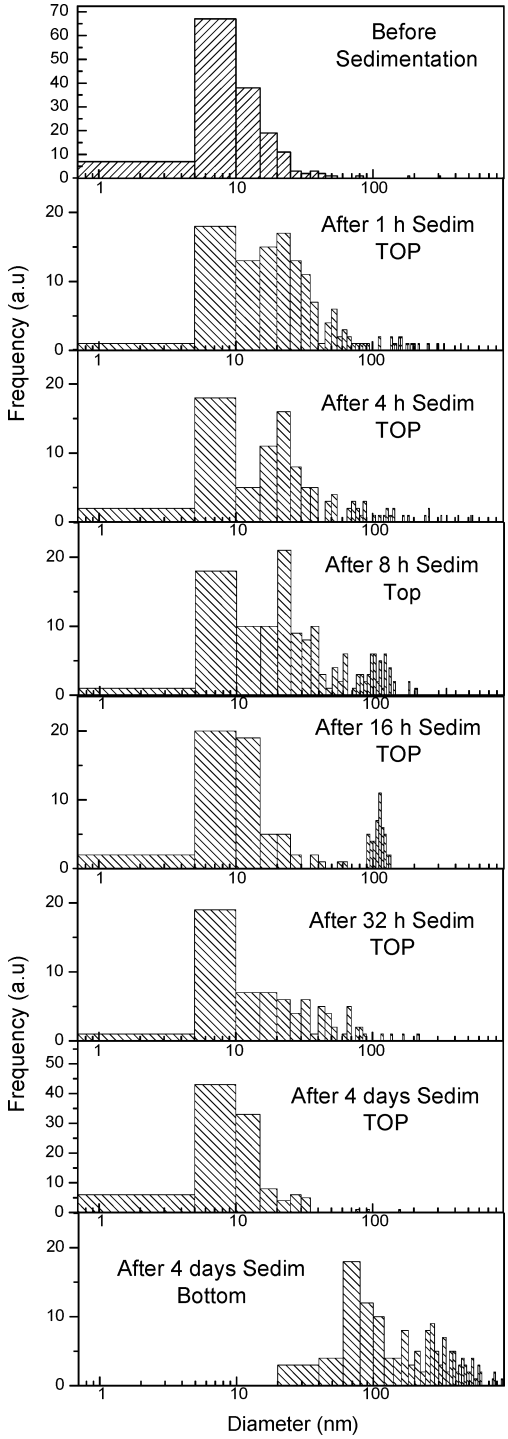

Figure 6. Histograms of bundle diameters for material pipetted from the top of the sample vessel after various sedimentation times. Note that the population of small bundles centered on 7.5 nm is observed at all times. A new population of larger diameter bundles begins to appear even after 1 h. Beyond 16 h this population disappears as the larger bundles sediment out of solution.

from the histograms that this population of small bundles exists at all times during the sedimentation. However, as time goes on a new population begins to build up at larger diameters. After 1 h the diameter distribution has already begun to spread to larger values. By 8 h, a significant group has formed in the region of 100 nm diameter. This group peaks at 16 h before decreasing with time as these larger diameter bundles sediment out of solution. After 96 h, the distribution has returned to its initial population, centered at 7.5 nm and extending to 35 nm. In comparison, the bundles in the sediment after 96 h have diameters varying from 30 to 1000 nm.

These results are extremely interesting. In the pristine $Mo_6S_{4.5}I_{4.5}$ powder, bundles are observed with diameters up to a few microns. However after sonication in 2-propanol this distribution collapses into a relatively narrow one centered around 7.5 nm. This shows that intense sonication is a very efficient way to partially debundle $Mo_6S_{4.5}I_{4.5}$ nanowires. As sedimentation proceeds however, most of these small bundles self-assemble into larger bundles with diameters of order of 100 nm. However, the fact that a small diameter population of bundles is stable over 200 h is intriguing. This suggests that the smaller stably dispersed bundles are fundamentally different to the ones that eventually aggregate and sediment. If all bundles were the same, as aggregation is just a free energy minimization process, we would expect the diameter distribution to broaden and shift to higher diameters. The fact that the distribution is actually bimodal with a constant component points to fundamental differences between the components. Further work is underway to understand the nature of these differences.

Furthermore, the bundle lengths for each sedimentation time were analyzed separately for small diameter bundles (<30 nm) and large diameter bundles (>30 nm). In each case the bundle length varied from 2 to 20 microns. However, at all times the average lengths of both small and large diameter bundles were approximately equal within error. It is expected that random aggregation processes would result in aggregates of bundles with their long axes parallel but with random displacements of the bundle center points from each other. These data suggest however, that after initial aggregation they slide relative to each other to maximize their contact area. This is almost certainly a manifestation of energy minimization by maximization of (negative) binding energy. However, it should be pointed out that this is only possible in this system due to the low internanowire shear modulus.[19]

This observation allows us to clarify the sedimentation process. From the results above, it is clear that the first entities to sediment out of solution are the nanoparticle impurities. These particles are significantly larger when found in the sediment compared to before sedimentation suggesting aggregation during sedimentation. We can at least partly associate these materials with phase 1. Furthermore, after approximately 8 h, much of the nanowire material has aggregated into very large bundles which subsequently sediments out of solution. Again we can associate this material with phase 2. Finally the stable phase seems to be associated with smaller bundles with diameters and lengths in the ranges $4-20$ nm and $1-6$ μm, respectively.

4.2.3. High-Resolution TEM. The fact that small bundles of nanowires are stable in 2-propanol after sedimentation allows us to study their structure in more detail. To this end, high resolution TEM pictures of the bundles observed in isopropanol (Figure 7) were also taken to understand better their nature and morphology. In Figure 7 a we present a typical HRTEM picture of a bundle, which shows them as arrays of well-ordered single nanowires. This structure is very similar to that observed for bundles of single walled carbon nanotubes. Shown in Figure 7b is a close-up of one of the kinks discussed earlier. This reveals two different regions of curvature in this kink, a sharp bend and a region of shallower curvature. Further work is needed to understand the nature and properties of these interesting structures.

4.2.4. Concentration Dependence. To further understand the bundle morphology, TEM measurements similar to those described in the previous section were made, after sedimentation,

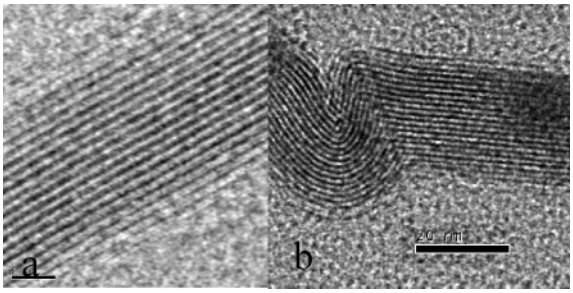

Figure 7. High-resolution TEM pictures of (a) a representative nanowire bundle and (b) of a kink. The scale bar in (a) is 5 nm while the scale bar in (b) is 20 nm.

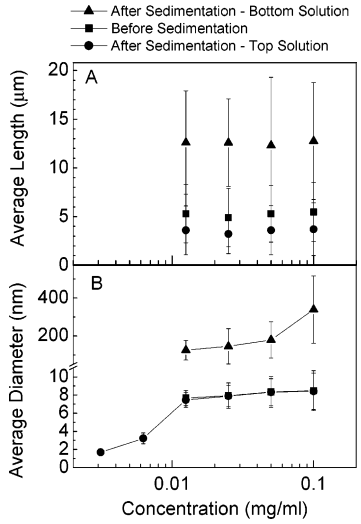

Figure 8. Average A) length and B) diameter of the nanowire bundles as a function of concentration in 2-propanol.

for a range of concentrations. For each concentration, the bundle size distribution was calculated by measuring diameters and lengths for over 300 bundles per sample. Diameters and lengths down to concentrations of 0.0125 mg/mL were measured by low resolution TEM and down to 1×10^{-3} mg/mL by HRTEM. These data are shown in Figure 8.

At concentrations down to 0.0125 mg/mL the bundle dimensions did not vary sifnificantly for the before and after sedimentation samples as well as the bundles observed in the sediment. Below 0.0125 mg/mL it was impossible to image bundles with the low resolution TEM, so instead HRTEM characterization was performed. At these lower concentrations the average bundle diameter fell dramatically to approximately 1.7 nm at 0.003 mg/mL. This diameter corresponds to bundles of two to three nanowires. This decrease in bundle size as concentration is decreased has also been reported for single wall carbon nanotubes.[7] However, very small bundles of only a few carbon nanotubes are only observed at very low concentrations. Due to experimental issues, it is of course very difficult to find and image individual nanowires at these low concentrations. However, by extrapolation we can estimate the concentration at which mainly individual nanowires would be found to be 1.5×10^{-3} mg/mL. This compares with the observation of individual carbon nanotubes in low concentration dispersions only at concentrations below 2×10^{-5} mg/mL.[7] Thus individual MoSI nanowires are stable at concentrations almost 100 times higher than are required to disperse individual carbon nanotubes. This result is very important as it shows that MoSI nanowires are not nearly as prone as carbon based systems to aggregation. This is in agreement with the fact that the inter-nanowire shear modulus and hence inter-nanowire interaction is significantly lower for molybdenum-sulfur based nanowires compared to carbon nanotubes.[19]

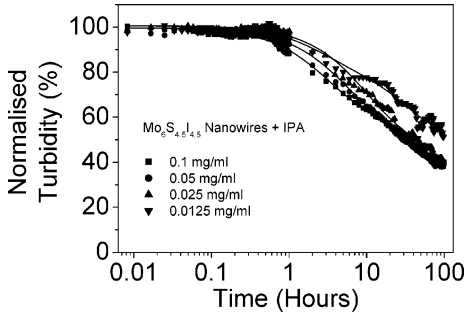

Figure 9. Experimental, normalized sedimentation curves (dotted lines) and biexponential fits (continuous lines) for $Mo_6S_{4.5}I_{4.5}$ nanowire bundles in 2-propanol in the range of concentration 0.1−0.0125 mg/mL.

4.3. Concentration Dependent Sedimentation Study. The data discussed in section 4.1 shows that a significant fraction of the nanowires are insoluble in all solvents. However, it is not clear why this is the case. There are two obvious possibilities. The first is that the MoSI bundles exist in two distinct types, one of which is dispersable and one of which is insoluble. The second possibility is that the partial concentration of stably dispersed nanowires, $C_0 = T_0/\alpha_0$, merely represents the maximum solubility at the concentration studied. To investigate this, sedimentation studies were carried out on dispersions of MoSI in 2-propanol at a range of concentrations from 0.1 to 0.0125 mg/mL. Below 0.0125 mg/mL it was found that the dispersion absorbance was too low to carry out sedimentation experiments.

The results of these experiments are shown in the form of normalized sedimentation curves in Figure 8 and fit parameters in Table 1. It is clear from these results that there is very little difference between the sedimentation properties of the dispersions in the concentration range studied. For the three higher concentrations, the fit parameters, T_0, T_1, T_2, t_1 and t_2, all agree within error. For the lowest concentration there is an increase in T_0 relative to the others from approximately 32% to 42%. However this is accompanied by a relative decrease in T_1 from approximately 32% to 20%. In addition for all concentrations T_2 stays in the 36−40% range. As T_1 represents the impurity phase, this means that a small fraction of impurities become soluble at 0.0125 mg/mL. However the fraction of insoluble bundles, represented by T_2, remains constant at all concentrations studied. This suggests that the insoluble nanowires are intrinsically insoluble and that T_0 does not just represent a concentration dependent solubility.

4.4. Sedimentation Studies on Polymer/$Mo_6S_{4.5}I_{4.5}$ Solutions. Many potential applications of MoSI nanowires involve composite formation. For carbon nanotube based systems, composite formation is generally carried out in solution.[4,7,8,12] While carbon nanotubes are insoluble in all solvents, they can be stabilized in solution by addition of a polymer. This possibility was tested for MoSI nanowires by addition of poly(vinylpyrrolidone) (PVP) in a range of MoSI/PVP mass ratios from 1:1 to 1:100. In all cases sedimentation experiments were carried out. The results of these experiments are shown in the form of normalized sedimentation curves in Figure 9 and fit parameters in Table 1. From the results in Figure 10 it is clear that the presence of PVP has a stabilizing effect on the dispersions at all mass ratios. The most apparent effect is the increase in T_0 as more PVP is added. This trend is shown more clearly in Figure 11.

However, a careful study of the fit parameters in Table 1 reveals that the increase in T_0 is accompanied by a decrease in

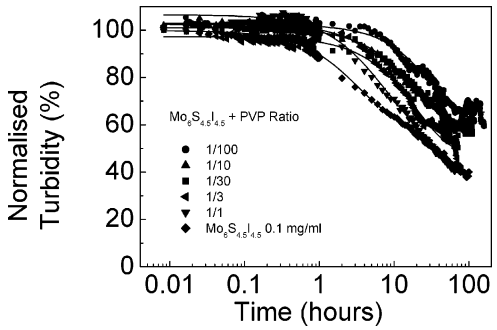

Figure 10. Experimental, normalized sedimentation curves (dotted lines) and biexponential fits (continuous lines) for $Mo_6S_{4.5}I_{4.5}$/polyvinylpirrolidone (PVP) dispersions in 2-propanol for different polymer/nanowires mass ratios.

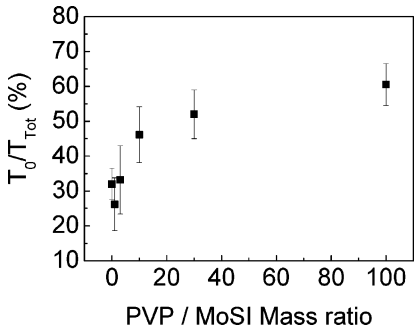

Figure 11. Partial turbidity of stably dispersed component as a function of PVP/MoSI mass ratio.

T_1 in addition to the expected decrease in T_2. This suggests that on addition of PVP both impurities and insoluble nanowires are being stabilized in solution.

This idea was tested by making a dispersion with MoSI/PVP mass ratio of 1:100, sedimentating and removing the sediment by decantation. The polymer was removed then by washing in a Buchner funnel.[8] The resulting MoSI powder was then redissolved in 2-propanol and examined using TEM. As expected, substantial amounts of spherical nanoparticulate impurities were observed confirming the stabilization of the impurity phase by the addition of PVP.

However the main result here is that PVP does not destabilize MoSI nanowires in 2-propanol. This means that composite formation in solution is feasible. In addition the sedimentation time constant for impurities is significantly shorter than that for insoluble nanowires. This means that the material can be purified by sedimentation in 2-propanol and then decantation with minimum loss of the insoluble nanowires. A suitable polymer could then be added to stabilize the insoluble nanowires and hence maximize the yield of nanowires in the composite solution.

5. Conclusions

In conclusion, sedimentation studies, involving the measurement of local particulate turbidity as a function of time, have been carried out on dispersions of $Mo_6S_{4.5}I_{4.5}$ nanowires in a range of solvents. Some degree of sedimentation was observed for all solvents. Theoretical considerations show that the local concentration of a given phase of dispersed particles decays exponentially with time with a time constant specific to that phase. Fitting the experimental sedimentation curves to the theory shows that the $Mo_6S_{4.5}I_{4.5}$ material consists of three phases, two of which are insoluble with one stable phase. TEM studies show that the insoluble material consists of spherical impurities and bundles of nanowires. The stably dispersed material consists of nanowire bundles that tend to be of smaller diameter and length compared to their insoluble counterparts. The impurity phase sediments out of solution with a time constant of between 15 min and 6 h, depending on the solvent, resulting in efficient purification of the material. Microscopy and spectroscopy show that while phase 1 is indeed associated with impurity material, both phase 2 and the solute consist mainly of nanowires. Quantitative analysis shows that after purification, concentrations of up to up to 0.34 mg/mL can be obtained in the best solvents. These were found to be 2-propanol and DMF. Microscopy studies showed that, in the case of 2-propanol, sonication significantly reduced the bundle size relative to the unsonicated bulk. However, during sedimentation, a large number of bundles were observed to reaggregate to form larger bundles which subsequently sedimented out of solution.

The sedimentation parameters, as found by fitting the experimental data, were not sensitive to the total sample concentration, indicating that the insoluble nanowire bundles are intrinsically so. However, TEM clearly shows that the stably dispersed bundle diameters decrease with concentration, until bundles of only two or three nanowires are observed at concentrations below 0.003 mg/mL. This is a reasonable high concentration considering that individual carbon nanotubes are stable only at concentrations below 2×10^{-5} mg/mg. It was found that the fraction of stably dispersed bundles could be increased on the addition of a stabilizing polymer. However this also resulted in the stabilization of some of the impurity phase. Nonetheless, stable polymer-nanowire dispersions were fabricated, opening the way for the formation of $Mo_6S_{4.5}I_{4.5}$ nanowire − polymer composites.

This work clearly shows that $Mo_6S_{4.5}I_{4.5}$ nanowires can form stable dispersions at reasonably high concentrations with the right choice of solvent. Furthermore, these materials are not nearly as susceptible to bundling as their carbon based counterparts. Coupled with their ease of synthesis and their monodisperse metallic nature, these results suggest that these materials are superior to carbon nanotubes in a range of areas. We anticipate that these inorganic nanowires will replace carbon nanotubes as the material of choice in areas from high strength, conductive fillers for composites to vias or interconnects in integrated nanoelectronics.

Acknowledgment. The authors wish to acknowledge the support of the European Union in the form of the European Community's Human Potential Program under contract HPRN-CT-2002-00192 [NANOTEMP]. J.N.C. and W.J.B. also wish to thank Science Foundation Ireland and the Irish Higher Educational Authority for financial support.

References and Notes

(1) Iijima, S. *Nature* **1991**, *354*, 56−58.

(2) Zaric, S.; Ostojic, N G.; Kono, J.; Shaver, J.; Moore, V. C.; Strano, M. S.; Hauge, R. H.; Smalley, R. E.; Wei, X. *Science* **2004**, *304*, 1129−1131.

(3) Dalton, A. B.; Collins, S.; Munoz, E.; Razal, J. M.; Von Howard, E.; Ferraris, J. P.; Coleman, J. N.; Bog, G. K.; Baughman, R. H. *Nature* **2003**, *423*, 703−704.

(4) Cadek, M.; Coleman, J. N.; Ryan, K. P.; Nicolosi, V.; Bister, G.; Fonseca, A.; Nagy, J. B.; Szostak, K.; Béguin, F.; Blau, W. J. *Nano Lett.* **2004**, *4*, 353−357.

(5) Duesberg, G. S.; Graupner, R.; Downes, P.; Minett, A.; Ley, L.; Roth, S.; Nicoloso, N. *Synthetic Metals* **2004**, *142* (1−3), 263−266.

(6) O'Connell, M. J.; Bachilo, S. M.; Huffman, C. B.; Moore, V. C.; Strano, M. S.; Haroz, E. H.; Rialon, K. L.; Boul, P. J.; Noon, W. H.; Kittrell, C.; Ma, J. P.; Hauge, R. H.; Weisman, R. B.; Smalley, R. E. *Science* **2002**, *297* (5581), 593−596.

(7) Coleman, J. N.; Fleming, A.; Maier, S.; O'Flaherty, S.; Minett, A. I.; Ferreira, M. S.; Hutzler, S.; Blau, W. J. *J. Phys. Chem. B* **2004**, *108*, 3446−3450.

(8) Murphy, R.; Coleman, J. N.; Cadek, M.; McCarthy, B.; Bent, M.; Drury, A.; Barklie, R. C.; Blau, W. J. *J. Phys. Chem. B* **2002**, *106*, 9, 2210−2216.

(9) Bachilo, S. M.; Strano, M. S.; Kittrell, C.; Hauge, R. H.; Smalley, R. E.; Weisman, R. B. *Science* **2000**, *298* (5602), 2361−2366.

(10) Chen, Z. H.; Du, X.; Du, M. H.; Rancken, C. D.; Cheng, H. P.; Rinzler, A. G. *Nano Lett.* **2003**, *3* (9), 1245−1249.

(11) Krupke, R.; Hennrich, F.; von Lohneysen, H.; Kappes, M. M. *Science* **2003**, *301* (5631), 344−347.

(12) Blake, R.; Gun'ko, Y. K.; Coleman, J. N.; Cadek, M.; Fonseca, A.; Nagy, J. B.; Blau, W. J. *J. Am. Chem. Soc.* **2004**, *126*, 10226−10227.

(13) Tenne, R. *Chem. Eur. J.* **2002**, *8*, 23, 5296−5304.

(14) Tenne, R.; Margulius, L.; Genut, M.; Hodes, G. *Nature* **1992**, *360*, 444−446.

(15) Remskar, M.; Skroba, Z.; Cleton, F.; Sanjines, R.; Levy, F. *Appl. Phys. Lett.* **1996**, *69*, 351−354.

(16) Remskar, M., Mrzel, A.; Skraba, Z.; Jesih, A.; Ceh, M.; Demsar, J.; Stadelmann, P.; Levy, F.; Mihailovic, D. *Science* **2001**, *292*, 479−481.

(17) Vrbanic, D.; Remskar, M.; Jesih, A.; Mrzel, A.; Umek, P.; Ponikvar, M.; Jancar, B.; Meden, A.; Novosel, B.; Pejovnik, S.; Venturini, P.; Coleman, J. C.; Mihailovic, D. *Nanotechnology* **2004**, *15*, 635−638.

(18) Nemanic, V.; Zumer, M.; Zajec, B.; Pahor, J.; Remskar, M.; Mrzel, A.; Panjan, P.; Mihailovic, D. *Appl. Phys. Lett.* **2003**, *82*, 25, 4573−4575.

(19) Kis, A.; Mihailovic, D.; Remskar, M.; Mrzel, A.; Jesih, A.; Piwonski, I.; Kulik, A. J.; Benoit, W.; Forro, L. *Adv. Mater.* **2003**, *15*, 9, 733−736.

(20) Tory, M. *Sedimentation of small particles in a viscous fluid*; Southampton Computational Mechanics, 1996.

(21) Burger, R.; Evje, S.; Karlsen, K H.; Lie, K. A. *Chem. Eng. J.* **2000**, *80*, 91−104.

(22) Garrido, P.; Concha, F.; Burger, R. *Int. J. Miner. Process* **2003**, *72*, 57−74.

(23) Atkins, P. W. *Physical Chemistry*, 4th ed.; Oxford University Press: 1992.